

Study on dynamic behavior of a new type of two-way single layer lattice dome with nodal eccentricity

Eka Satria*, Shiro Kato, Shoji Nakazawa and Daisuke Kakuda

*Dept. of Architecture and Civil Engineering, Toyohashi Univ. of Technology
Tempaku-cho Azahibarigaoka1-1, Toyohashi, 441-8580, Japan*

(Received September 23, 2008, Accepted November 10, 2008)

Abstract. This paper discusses a feasibility of a new type of two-way system for single layer lattice domes with nodal eccentricity by investigating the dynamic behavior under earthquake motions. The proposed dome is composed of two main arches, intersecting each other with T-joint struts to provide space for tensioning membranes. The main purposes of this study are to calculate the nonlinear dynamic response under severe earthquake motions and to see the possibility of using this new type of two-way system for single layer lattice domes against earthquake motions. The results show that the main arches remain elastic except yielding of the joints of strut members that can be used to absorb some amount of strain energy at strong earthquake motion. Consequently, deformation of the main arches can be reduced and any heavy damages on the main arches can be minimized. A kind of damage-control characteristic appeared in this system may be utilized against severe earthquake motions, showing a possibility of designing a new type of single layer lattice dome.

Keywords: earthquake response; lattice dome; single layer; two-way; nodal eccentricity; damage controller.

1. Introduction

The two-way system for single layer lattice domes is attractive to architects and engineers since such a system is beautiful in shape, light in weight, simple in geometry and systematic in construction. Some researches have been previously conducted in this area, such as the newest one done by Kato *et al.* 2007, focused on design method of dome against buckling failures based on the column buckling concept. However, nowadays in order to fulfill artistic design purposes, double layer steel lattice roofs are being frequently used as large span structures. Some of them, such as Akita-Sky Dome in Japan, Sports Palace Dome in Mexico, and Velodrome of Dos Hermanas in Spain; have employed a steel two-way network to support their membrane roofs that have been kept in shape by introducing tensions by cables or slender bars. For application of these tensions, an amount of different height has been prepared using some kind of struts or bracing elements located above or within the roof. Akita Sky Dome has adopted a set of two-way arches, and the system is realized as a double layer system using vierendeel arches in one direction and vertically braced arches in its orthogonal direction (Kurokawa *et al.* 1988, Ishii 1995). Sports Palace Dome with roof surface like spherical shell was built as a two-way grid of steel trusses forming intersecting arches. The square areas between the arches were filled by triangular grid of

*Corresponding Author, Email: satria_eka@st.tutrp.tut.ac.jp

tubular aluminium single layer hyperbolic paraboloidal units (Fentiman 1984, Narayanan 2006). Velodrome of Dos Hermanas has employed a two-layer curved grid supported on four piers placed in the corners of square edges. The roof's meshing of two-way system is formed by two intersected vierendeel arches (Escrig *et al.* 2001, 2004). However, the system for tensioning membranes is often required to have a more complex structural system with many sub-members. Therefore, due to cost consideration, the structural system should be made simple, like a single layer system.

To follow the trend of modern design with aesthetical appearances and easiness in construction, this present paper introduces a new type of two-way system for single layer lattice dome. The model is composed of two main arches intersecting each other with T-joint struts, as shown in Fig. 1a, to provide a space for tensioning membranes. The global form becomes simple because of the use of these T-joint struts. The difference from the previous models is that the system adopts no diagonal bracing elements to avoid complications in construction.

The previous task of the researches investigated the buckling behavior of the proposed dome under vertical static loads such as snow loads (Kato *et al.* 2007, 2008, and Satria *et al.* 2008). The study showed the feasibility of applying the model in non-seismic area by comparison of the critical design loads of the proposed dome with the magnitude of design loads for similar and ordinary type of lattice domes. Another remarkable finding in the studies was its self recovery system at large displacements that would occur due to heavy snow loading. The mechanism of this recovery was found due to the fact that most of the deformations attribute to the elastic strains in the structure at usual loading; and once an overload is given, some parts at the ends of strut members (joint connections) are deformed plastically without causing any notable damages to the main arches.

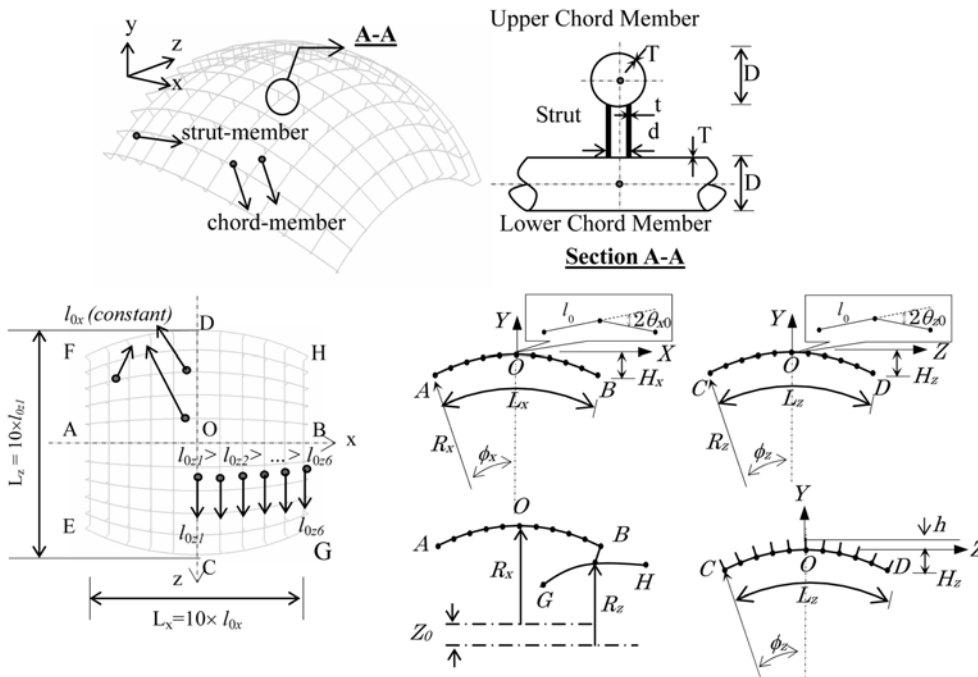


Fig. 1(a) Two-Way Single Layer Lattice Dome with Nodal Eccentricity (upper) (b) Configuration of Dome: Geometrical Model (lower-left) and Geometrical Parameters (lower-right).

This behavior is considered to be beneficial when the dome is loaded by dynamic loads such as earthquake motion. Input energy is possibly absorbed by the joint yielding of the strut members reducing the earthquake damages, especially to the main arches of the dome. This hypothesis could be a kind of improvement of behavior of structures based on energy concepts which recently has been a matter of great concern. Apart from a brief review about seismic dissipation devices of steel and composite structures given by Soong *et al.* 2002 and Di Sarno *et al.* 2005, there are still limited numbers of researches that propose a new configuration which can directly behave like a damage controller under earthquake, especially for single layer lattice domes. In many cases, some devices such as pendulum isolator (Tatemichi *et al.* 2000), lead rubber bearing (Hitomi *et al.* 2001), viscous damper (Fan *et al.* 2004), J-shape friction damper (Kato *et al.* 2006), *etc.* are installed at support to reduce the effect of earthquake load to the dome structures, Only a few studies were proposed based on energy dissipation through inelastic deformation. For examples, Kato *et al.* 2000 presented a seismic design concept for the single layer lattice dome supported by a substructure composed of steel braces and column, by means of yielding of the braces. This configuration later was combined by installation of visco-elastic damper into braces to reduce the earthquake damages (Kato *et al.* 2001). Fujita *et al.* 2002 proposed structural types of axial yield hysteretic dampers for flat system truss as a damage-controlled structure. From evaluation for performance, it was suggested that the proposed type is feasible to apply for the large span structures. Other bracing configurations with a modification was then proposed by several researchers, such as Ciampi *et al.* 1990, Jurukovski *et al.* 1995 and Sabouri-Ghomi *et al.* 2005 through application of a closed frame with four connected edges to concentrically braced frame. The central system in this configuration acts as energy absorber that was designed to yield in serious and medium earthquakes. Out of field of spatial structures, this kind of mechanism could also be found in design of beam-column connection. In controlling any unexpected damages on column, some designers often make a weakening part in beam sections such as reduction of beam section (Jin *et al.* 2005), web opening (Satish Kumar *et al.* 2006), wedge design (Wilkinson *et al.* 2006), *etc.* to act as energy absorber under earthquake. The purpose is to reduce plastic capacity of the beam and induce the plastic hinge at these weakened parts at heavy loads.

This paper is focused on two main purposes; firstly, to evaluate the feasibility of the single layer dome with the proposed joint system in seismic region, secondly, to see a possibility of the joint yielding characteristic that can behave as a damage control mechanism under medium or strong earthquakes. To achieve the purposes, some studies which cover several dynamic aspects, such as a description of typical major vibration modes under horizontal earthquake, total maximum displacement and acceleration of the dome under various earthquake intensities, internal forces and distribution of the absorbed energy on each member, shear deformation, and residual plastic deformation, are conducted. From the results, the feasibility of the proposed dome to be built in seismic area and the effectiveness of joints as energy absorber under earthquake are justified.

2. Numerical modeling

2.1 Configuration of dome

As shown in Fig. 1b, the network is two-way and the dome is composed of a set of parallel arches, and each arch is connected through a set of struts to the orthogonal arches. In the analysis, the surface of the roof is assumed like a curved shell, which is formed geometrically by rotating an arch of *AOB* with

a radius R_z along the two same shaped arches of EAF and GBH . The radii of arches AOB and COD are R_x and R_z respectively. The total rise H is the sum of the rise, H_z , for the arch in the z direction, the length of the strut, h_t , and the diameter of the chord, D , or mathematically written as $H = H_z + h_t + D$. The length of each member along the arches AOB and COD might be an arbitrary. In Fig. 1b, several parameters are also introduced. Firstly, h_t is assumed to be constant, 250 cm. Secondly, l_0 is the length of arch member for each division has been assumed to be constant of 600 cm at the centre of the dome in x and z direction. The surface has two half open angles, f_x and f_z , respectively in the x and z directions. In this paper ϕ_x and ϕ_z are assumed 30° and 25° . Then, each arch is divided into n members, n being assumed as 10 in this study, and the total arc lengths, L_x and L_z are set just to be 6,000 cm. Therefore, both radii of arches can be calculated through equations, $R_x = n.l_0/2\phi_x = 5729.6$ cm and $R_z = n.l_0/2\phi_z = 6875.5$ cm, and the difference, $Z_0 = R_z - (R_x - h_t) = 1395.9$ cm using $h_t = 250$ cm.

2.2 Geometrical and material properties of tubular member

Tubular T-joint is modeled by connecting arch member, with diameter $D = 318.5$ mm and thickness $T = 8$ mm, to strut member, with diameter $d = 216.3$ mm and thickness $t = 8$ mm. Both members are made of steel using modulus of elasticity (E) is 205×10^3 N/mm² and yield stress (s_y) is 235 N/mm².

2.3 Rigidity and strength of joints

Rigidities and strengths of the tubular T-joint are determined by Recommendation Design of Steel Tubular Structure published by Architectural Institute of Japan (AIJ) 1990, under three types of loading; in-plane bending (IPB), out-of-plane bending (OPB) and axial loading (AXL). In Table 1, the rigidities and strengths of T-joint are provided as follows.

In the numerical analysis of two-way single layer lattice domes, it is common to model their members using beam elements which interact to spring elements as their joint connections. A tri-linear model is considered to approach the loading-displacement relationship at the joints, based on works done by Kato *et al.* and Satria *et al.* 2007, 2008. This model is accurate enough and easy to apply in numerical modeling. In space frame model, the tri-linear model can be assembled by superposition of two bi-linear springs with difference values of rigidities and strengths, as illustrated in Fig. 2. The relationship of the rigidities between those two springs and tri-linear model can be mathematically expressed in Eqs.(1) and (2). Here, M_y and M_u represent the yield moment and ultimate moment of the joint respectively (based on Table 1), while K_I and K_{II} represent the bending rigidity of arranged spring-I and spring-II. The notation θ_{yI} means the yield rotation of spring-I which is equal to the yield rotation of joint θ_y , while θ_{yII} means the yield rotation of spring-II which is equal to ultimate rotation of joint θ_u (see Fig. 2). Note that K and dK represent the first and second slope of rigidities of the joint in terms of tri-linear model, which have been determined previously based on design equations of AIJ Recommendations. Here, dK is defined as $dK = K/20$ for bending cases and $dK = K/5$ for axial loading cases as suggested by Kato *et al.* and Satria *et al.* 2007, 2008.

Table 1. Rigidities and Strength of T-Joints

$K_{IPB} (\times 10^4)$ (N.mm/rad)	$K_{OPB} (\times 10^4)$ (N.mm/rad)	$K_{AXL} = AE/L$ (N/mm) ($\times 10^2$)	$M_{y,IPB} (\times 10^4)$ (N.mm)	$M_{u,IPB} (\times 10^4)$ (N.mm)	$M_{y,OPB} (\times 10^4)$ (N.mm)	$M_{u,OPB} (\times 10^4)$ (N.mm)	$P_{y,AXL} (\times 10^3)$ (N)	$P_{u,AXL} (\times 10^3)$ (N)
572589.62	120666.19	4455.43	3724.50	5313.62	1125.89	1606.27	128.34	183.10

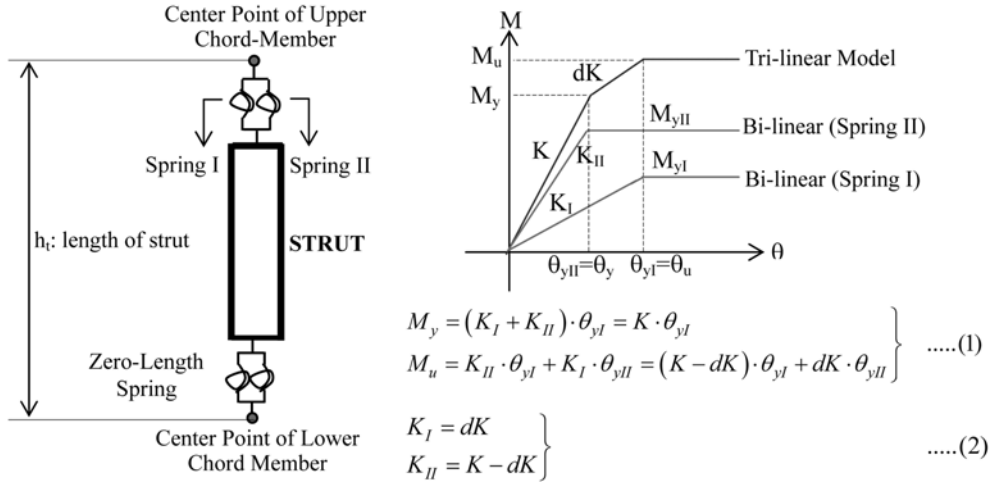


Fig. 2. Modeling of Joint Connection: Tri-Linear Model

2.4 Boundary condition and distribution of dead load

The dome is assumed to be initially subjected to a vertical dead load, given by summation of weight of roof and weight of material, at the upper and lower node of the strut members. Arches at the boundaries where all strut nodes have to be pin-supported (restrained in the x , y and z directions) at their upper and lower joints are exempted.

2.4.1 Distribution of roof weight

The dome is assumed capable to support a roof weight around $w_{dead,1} = 60 \text{ kgf/m}^2 \approx 0.59 \text{ kN/m}^2$ for area of “ A_s ” ($A_s = 6 \times 6 = 36 \text{ m}^2$). It means that the load per one node will be $P_{dead,1} = w_{dead,1} \times A_s \times (1/2) = 10.62 \text{ kN/node}$. Here the factor (1/2) is adopted to calculate one nodal load out of two nodes located at the upper and lower joints of the strut members at a given area “ A_s ”. As the proposed model have a total number of 423 nodes, which consist of 162 nodes at the joint positions and 261 nodes at the middle of members, the total load given to nodes at joint positions is equal to $P_{total,dead,1} = 162 \times 10.62 = 1,720 \text{ kN}$. Further, it is assumed that only 80% of $P_{dead,1}$ is distributed to the nodes at the joint positions and the rest is uniformly distributed to the middle of members; therefore

- Load per each node at the joint position, $P_{N1,dead,1} = 0.8 \times 10.62 = 8.5 \text{ kN}$
- Load per each node at the middle of member, $P_{N2,dead,1} = (P_{total,dead,1} - P_{N1,dead,1} \times 162)/261 = 1.31 \text{ kN}$.

2.4.2 Distribution of material weight

The density of steel (ρ_s) is assumed 7.86 tons/m^3 ; the mass (m_s) can be determined by multiplication of density (ρ_s) and member volume (V). Therefore a self-load per each node can be calculated as follows.

- Load per each node at the joint position, $P_{N1,dead,2} = 7.86 \times (80.05 \times 10^{-6} \times 300) \times 9.81 + 7.86 \times (54.36 \times 10^{-6} \times 125/2) \times 9.81 = 2.12 \text{ kN}$.
- Load per each node at the middle of the arch member, $P_{N2,dead,2} = 7.86 \times (80.05 \times 10^{-6} \times 300) \times 9.81 = 1.85 \text{ kN}$.
- Load per each node at the middle of the strut member, $P_{N2,dead,3} = 7.86 \times (54.36 \times 10^{-6} \times 125) \times 9.81 = 0.52 \text{ kN}$.

2.4.3. Total Weight

The total load per node at the joint position will be $P_{TOT-DEAD,1} = 8.5 + 2.12 = 10.62$ kN; then load per node at the middle of the arch members will be $P_{TOT-DEAD,2} = 1.31 + 0.52 = 1.83$ kN, while load per node at the middle of the strut members will be $P_{TOT-DEAD,3} = 1.31 + 1.85 = 3.16$ kN (see Fig. 3).

2.5. Typical earthquake ground motion

The acceleration of input earthquake motion used in this analysis is El-CentroNS(1940). Actually any type of recorded earthquake motion is possible to use, but the reason of this El-CentroNS (1940) was only due to that it often uses by many researchers all over the world. This earthquake ground motion data, as seen in Fig. 4, is later applied to the proposed dome in horizontal x and z directions.

3. Static elasto-plastic analysis

Since the effects of geometrical imperfections on buckling load capacity are significant in single layer lattice domes (Kato *et al.* 2002, 2005, Lopez *et al.* 2007, Balut *et al.* 2000), the present study assumes a distribution $W_{imp}(x,z)$ for geometrical imperfection based on the first buckling mode obtained by FEM eigenvalue analysis as shown in Fig. 5. Then normalization of deformation is adopted, so that the peak value of $W_1(x,z)$ to be 1.0 for the maximum deflection.

$$w_{imp}(x,z) = wi_0 \cdot W_1(x,z); wi_0 = \pm \min(L_x/1000, L_z / 1000) \tag{3}$$

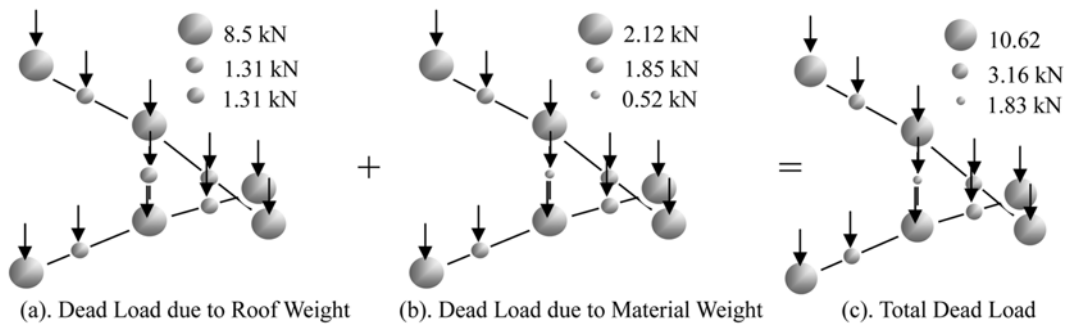


Fig. 3 Distribution of Dead Load

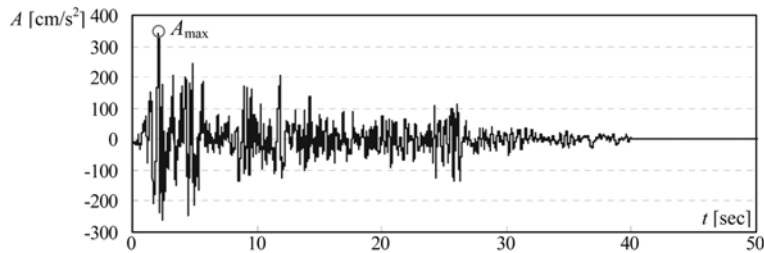


Fig. 4 Input Acceleration of El-CentroNS (1940)

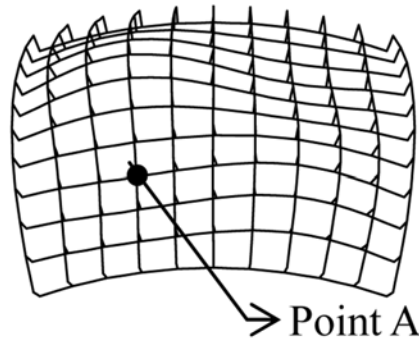


Fig. 5 Geometrical Imperfection based on the first buckling mode

The maximum amplitude of imperfection w_{i0} of the proposed dome is limited to be 6.00 cm in y direction. The limiting value was resulted from Eq.(3) provided by JASS Steel Work 1993 for the span of 60 m. A uniform vertical load is considered to be applied to joint positions only (excluding restrained joints at boundaries) as described in Section 2.4. Therefore, by dividing the total dead load from the number of joints the static dead load per one node will be $P_0 = 15.55$ kN/node or $w_0 = 2 \times P_0/A_s = 0.86$ kN/m².

Fig. 6 shows the static load-displacement response of the dome under elastic and elasto-plastic analysis. The critical buckling load is determined as $P_{cr}^{el} = 56.56$ kN/node ($3.64 \times P_0$) from elastic analysis, and $P_{cr}^{el-pl} = 37.89$ kN/node ($2.43 \times P_0$) from elasto-plastic analysis in which the yielding of the strut joint started at $P = 32.65$ kN/node ($2.1 \times P_0$). This analysis uses the criteria specified in Design Standard for Steel Structures published by AIJ 2002. It notifies that the maximum displacement under the critical load from elastic analysis should be less than or equal to $\delta_{max} = L_z/300 = 6000/300 = 20$ cm. It means the load that gives $\delta_{max} = 20$ cm can be notified as the critical load. This is found as $P_{cr}/P_0 = 2.06$ leading $P_{cr} = 31.1$ kN/node or in term of load intensity, $p_{cr,design} = 2 \times 31.1$ kN/(6×6 m²) = 1.73 kN/m². The fact proves that, practically the dome can be used to support the dead load (0.86 kN/m²) and additional vertical load other than the dead load, like a snow load up to 0.87 kN/m² corresponding to regions under moderate snow loads in Japan.

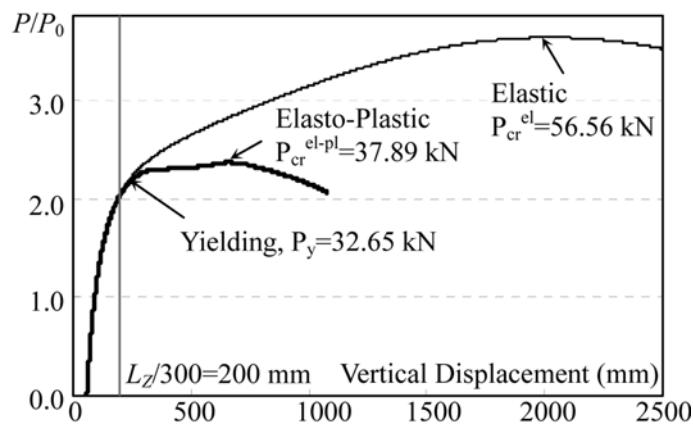


Fig. 6 Static Response of Loading-Displacement (Ref. Point: A)

4. Dynamic elasto-plastic analysis

Methods for dynamic analyses are the linear eigenvalue analysis and dynamic response analysis which takes into account the nonlinearities of geometry and material. Eigenvalue analysis determines the major deformation modes for vibration, while the elasto-plastic dynamic analysis describes the nonlinear behavior of the domes under earthquake motions.

4.1 Linear eigenvalue analysis

The major vibration modes of the proposed dome are selected based on effective modal mass ratio (ρ_i) and input energy (E_{inp}) which is determined through Eq. (4) below.

$$E_{inp} = \frac{1}{2} \cdot \rho_i \cdot m_T \cdot Sv_i^2 \quad (4)$$

where m_T is the total mass determined from w_{tot}/g (kg), and Sv is the velocity response of the selected mode (cm/s). Effective modal mass ratio (r_i) is defined as the ratio of the effective modal mass of i -th mode to the total mass in a direction of earthquake motion. Using input earthquake motion EI-CentroNS with maximum input acceleration $A_{max} = 341 \text{ cm/s}^2$, the velocity responses spectra for damping factor of $h = 2\%$ is determined by applying Newmark method with $\beta = 1/4$.

Based on the input energy for two directional horizontal motions (x and z directions), we limit our focus only on modes that have their natural vibration period between 0.1 sec. (225^{th} mode) and 1.5 sec. (1^{st} mode). All other modes above 225^{th} have got insignificant effective mass and small input energy. The highest effective mass under motion in the x direction occurs at the 30^{th} mode with natural periods around 0.35 sec. , while the highest effective mass under motion in the z direction occurs at the 10^{th} mode with natural periods around 0.45 sec. (see Figs. 7 and 8).

Fig. 7 shows that the deformations occurred at major mode under x directional earthquake motion are non-symmetric; and nodes at the upper arches seem to be largely deformed in the horizontal x direction, while nodes at the lower arches are mainly deformed in the both x and z directions. The deformations at major mode under the z directional earthquake motion, as seen in Fig. 8, seem to be symmetric in the z direction but not in the x direction. The deformed shapes in the x and y directions are dominant than in the z direction (the direction of earthquake motion).

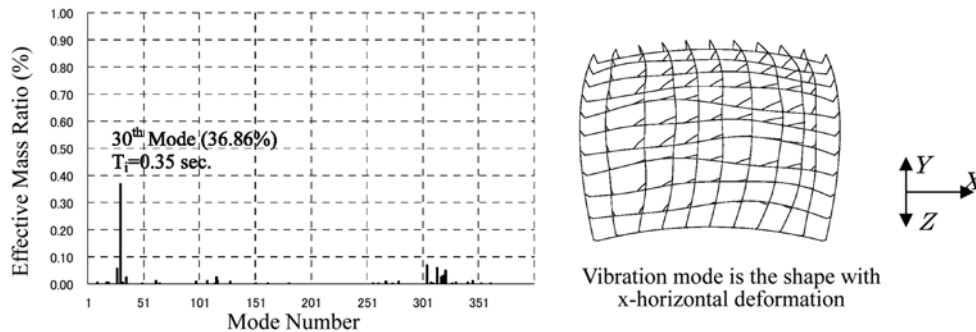


Fig. 7 Effective Mass Ratio vs Modes under earthquake motion in x-direction

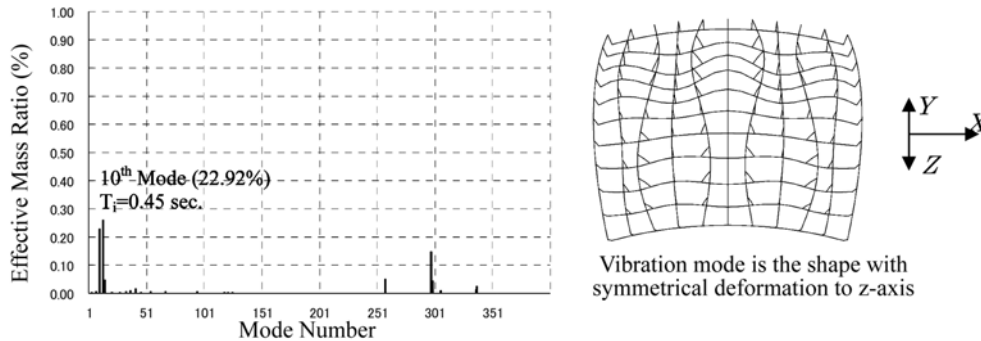


Fig. 8 Effective Mass Ratio vs Modes under earthquake motion in z-direction

4.2. Elasto-plastic dynamic analysis

In nonlinear elasto-plastic dynamic analysis, the earthquake motion with maximum acceleration (A_{max}) which is varied between $A_{max} = 0 \text{ cm}^2/\text{s}$ to $A_{max} = 500 \text{ cm}^2/\text{s}$ is applied to the proposed dome in x or z direction and some behavior is described in the following sections. Newmark method with $\beta = 1/4$ is adopted for numerical analysis. The dead load is applied quasistatically with a critical damping factor $h = 1.0$ during the time t ranging from 0.0 to 20.0 sec with increment $\Delta t = 0.05 \text{ sec}$. Subsequently the dynamic load is added for 60 sec. with a damping factor $h = 0.02$ as Rayleigh damping for the natural periods of $T_1 = 1.5 \text{ sec}$. and $T_2 = 0.1 \text{ sec}$.

4.2.1. The selected arches

Several arch members of the dome are labeled as in Fig. 9 for result clarification. The left upper arch is marked by number ① - ①' and the right upper arch is marked by number ⑨ - ⑨' (arches on both side boundaries are exempted). The nonlinear behavior of the nodes at the upper arches, numbered ⑤ - ⑤', ⑦ - ⑦' and ⑨ - ⑨' are chosen to be observed in x , y , and z directions. Similar procedure is followed for the lower arches as shown in Fig. 9b, by labeling extreme bottom arch as $a - a'$ and the most top as $i - i'$; again arches at boundaries are omitted. The nonlinear behavior of the nodes at selected arches; $a - a'$, $c - c'$ and $e - e'$ are observed.

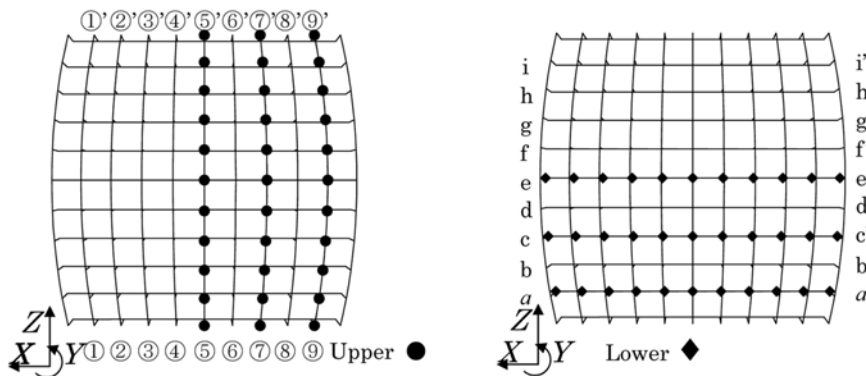


Fig. 9 The selected arches (a).Upper Arches (left) (b). Lower Arches (right)

4.2.2. Displacement under dead load

Fig. 10 shows the displacement responses of the selected nodes (as marked in Fig. 9) under the dead load ($P = P_0$) for three directions (x, y and z direction). The results show that the maximum displacement occurs in negative y -direction is around 10.4 mm for both upper and lower nodes of the strut member.

4.2.3. Nodal displacements

Fig. 11 shows the nodal displacements of the selected upper and lower arches under the earthquake excitation given in the x direction. It could be observed that the x directional displacements of upper arches are significant. In contrast, the y directional displacements are prominent in lower arches even for the selected maximum acceleration of the earthquake $A_{max} = 500 \text{ cm/s}^2$. For instance, under the x directional earthquake excitation $A_{max} = 500 \text{ cm/s}^2$, one node at the upper arch ⑨ - ⑨' has been largely deformed up to 81.51 mm in the x direction, while at the lower arches, one node at the arch $e - e'$ has been deformed to 32.8 mm in the y direction. Some reasons for these conditions are; (1) at the upper arches, the rigidity of joints in the x direction (OPB section) is smaller than in the z direction (IPB section). Therefore the earthquake load, which is also given in the weaker x direction, is able to displace nodes

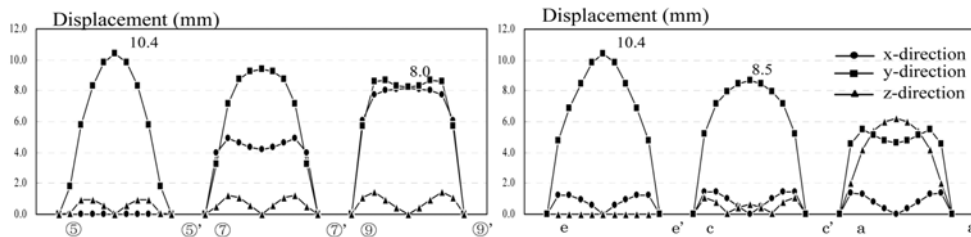


Fig. 10 Nodal Displacements of The Selected Arches under Dead Load ($P = P_0$); (a). Upper Arches (left) (b). Lower Arches (right)

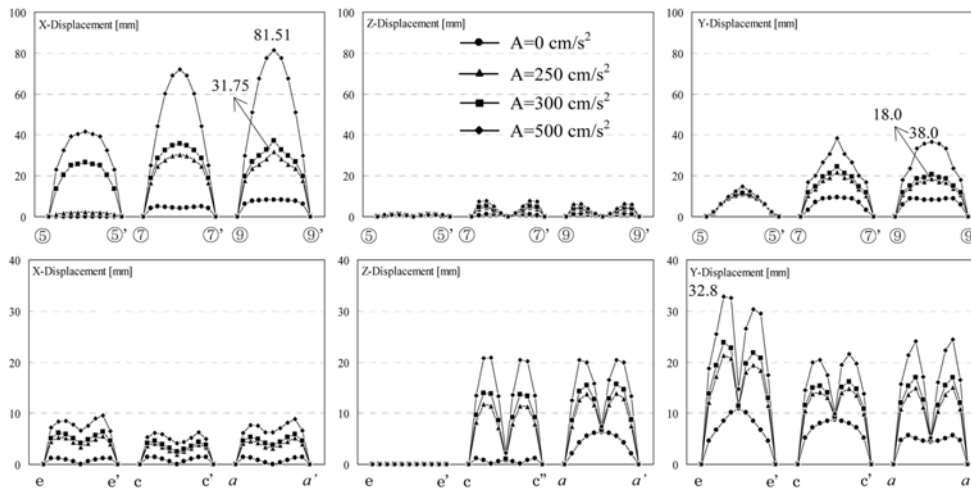


Fig. 11 Nodal Displacement of The Selected Arches under Earthquake Motion in the X Direction; (Upper: Left to Right) Upper Arches; X, Z, Y Displacement (Lower: Left to Right) Lower Arches; X, Z, Y Displacement

largely in the x direction rather than in the z direction, (2) at the lower arches, the rigidity of joints in the x direction (IPB section) is larger than in the z direction (OPB section). Therefore earthquake load given in the x direction is not strong enough to displace nodes largely in the x direction. In this case, the displacement occurred in the y direction due to effect of external load and the dead load is highlighted.

Fig. 12 shows the nodal displacements of the selected upper and lower arches under the earthquake motion given in the z direction. In this case, y displacements of nodes at upper arches are significant, while displacements of nodes at lower arches are substantial in the z and y direction. For the selected maximum acceleration of earthquake $A_{max} = 500 \text{ cm/s}^2$, maximum y directional deformation of 70.70 mm is observed at one node of the upper arch ⑦ - ⑦'. In the lower arches, one node at the arch $a - a'$ has been deformed 65.28 mm in the z direction and one node at the arch $c - c'$ has been deformed 73.97 mm in y direction. Some reasons for these conditions are; (1) at the upper arches, the rigidity of the joints in the z direction is larger than in the x direction. Therefore the earthquake load which is given in the z direction is not strong enough to displace nodes largely in the z direction compared to the x direction; but in the mean time, the effect of the dead load could make the y directional deformations become prominent (2) at the lower arches, the rigidity of the joints in the z direction is smaller than in the x direction. The earthquake load is become proficient to displace nodes easily in the z direction.

4.2.4 Nodal acceleration

Figs. 13 and 14 demonstrate responses of nodal acceleration of the selected arches under earthquake motion given in the x and z direction respectively. Generally, the results show the same tendency with nodal displacements that were previously described (see section 4.2.2).

4.2.5 Internal forces of member

From several preliminary analyses performed by Kato *et al.* 2007, 2008 and Satria *et al.* 2008, the

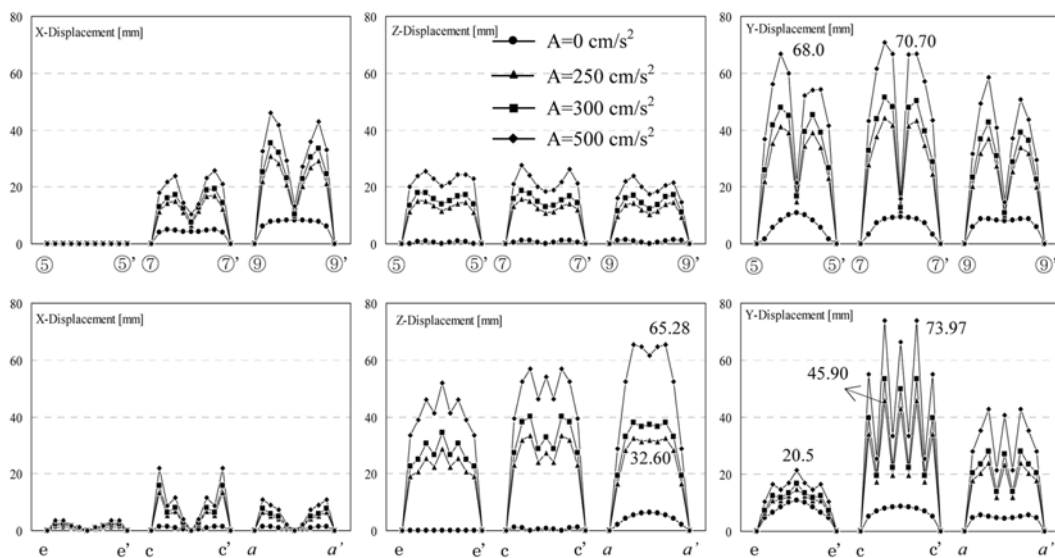


Fig. 12 Nodal Displacement of The Selected Arches under Earthquake Motion in the Z Direction; (Upper: Left to Right) Upper Arches; X, Z, Y Displacement (Lower: Left to Right) Lower Arches; X, Z, Ydisplacement

joint characteristics of the strut have been known to have a noteworthy effect on the overall behavior, since the strut members are used to connect the two main arches of the dome. Therefore, this section focusses on determining internal forces of the struts since the internal forces of the arches are very much lower than their yield points (in all types of loading) and therefore may be omitted. Strut members at the same arches shown in Fig. 9 are selected.

Fig. 15 shows the internal forces of the selected strut members in case of earthquake motion in the x direction. Results show that axial force has only a little effect on the yielding of the joints ($P_y = 128.24$ kN).

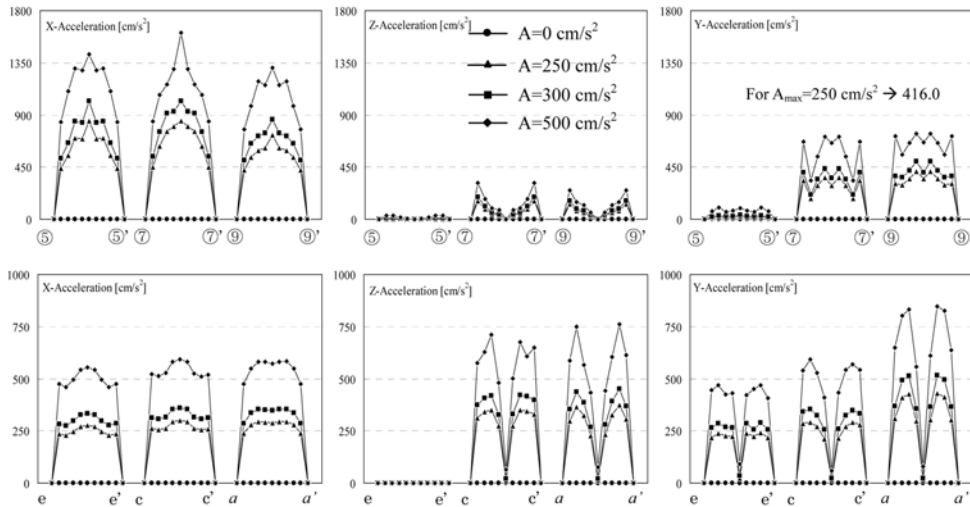


Fig. 13 Nodal Acceleration (cm/s^2) of The Selected Arches under Earthquake Motion in the X Direction; (Upper: Left to Right) Upper Arches; X, Z, Y Displacement (Lower: Left to Right) Lower Arches; X, Z, Y Displacement

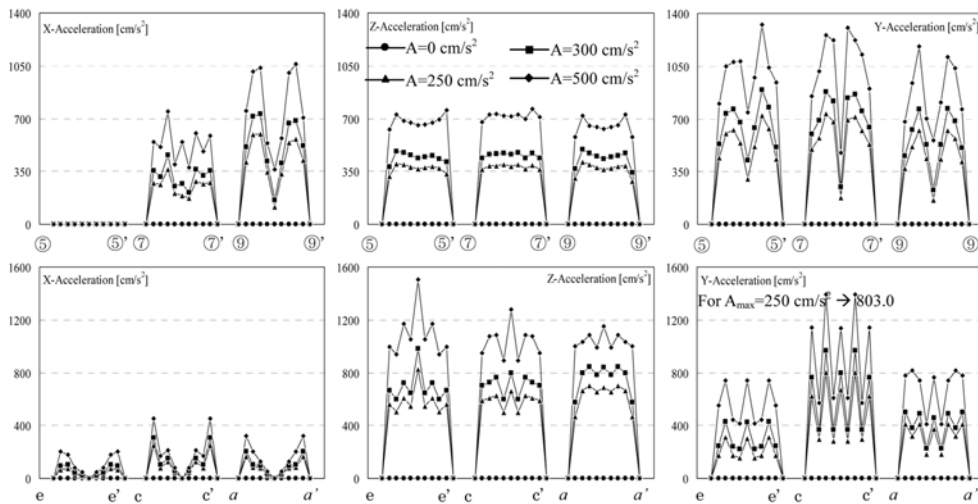


Fig. 14 Nodal Acceleration (cm/s^2) of the Selected Arches under Earthquake Motion in the Z Direction; (Upper: Left to Right) Upper Arches; X, Z, Y Displacement (Lower: Left to Right) Lower Arches; X, Z, Y Displacement

The maximum axial forces are much lower than the yielding load. As for bending, in-plane bending (*IPB*) moments are larger than out-of-plane bending (*OPB*) moments. The *IPB* at upper and lower joints are represented by M_y and M_z respectively. The maximum M_y for $A_{max} = 500 \text{ cm/s}^2$ is about 20.20 kN.m and has not reached the yield value ($M_{y,IPB} = 37.24 \text{ kN.m}$, as shown in Table 1). However, the maximum M_z is about 44.0 kN.m for $A_{max} = 500 \text{ cm/s}^2$, which is larger than the yield point. Therefore at earthquake motion with this A_{max} , the lower joint of this strut member is yielded.

Fig. 16 shows the internal forces of the selected struts under earthquake motion in the z-direction. From the results, the maximum axial forces do not reach to the yield joint ($P_y=128.24 \text{ kN}$). In bending cases, again the in-plane bending (*IPB*) moments are larger than the out-of-plane bending moments (*OPB*). The *IPB* at upper joint represented by M_y , becomes maximum ($M_y=41.6 \text{ kN.m}$) for $A_{max} = 500 \text{ cm/s}^2$ and exceeded the yield limit of the joint ($M_{y,IPB} = 37.24 \text{ kN.m}$). Also M_z , the *IPB* at lower joint reaches 36.5 kN.m for $A_{max} = 500 \text{ cm/s}^2$ and this is slightly lower than the yield point.

Several remarks that can be noticed from these outcomes are; (1) the *IPB* has a significant effect on failure of the T-joints, (2) for the given dome's dimension, explained in Section 2.1, the joint yielding of the strut members can be avoided if the earthquake motion acceleration A_{max} lower than 300 cm/s^2 , and (3) under loaded by the earthquake in the x direction, yielding of the lower joints become the focal point of the design as a large M_z appeared; while for the earthquake given in the z direction, failure of the upper joint is crucial with the emergence of a large M_y .

4.2.6 Absorbed Energy

Energy absorbing capability is determined by examining the dome under earthquake loadings with maximum acceleration A_{max} is varied between 0 to 500 cm/s^2 . Several types of energy then are evaluated. The consumed energy is summation between kinematics, damping and strain energy, as shown in Fig. 17. The kinematic energy is almost zero after the earthquake.

Table 2 and 3 show the exact values and also the percentage of strain energy absorbed by the arches

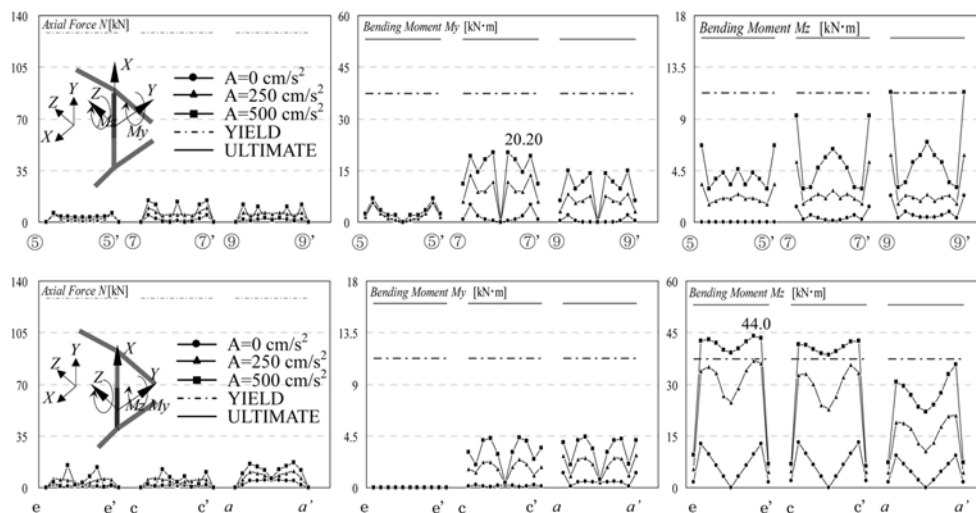


Fig. 15 Member Forces of The Selected Struts under Earthquake Motion in the X Direction; (Upper: Left to Right) Upper Joint of Strut; Axial Forces, Bending Moment M_y , Bending Moment M_z (Lower: Left to Right) Lower Joint of Strut; Axial Forces, Bending Moment M_y , Bending Moment M_z

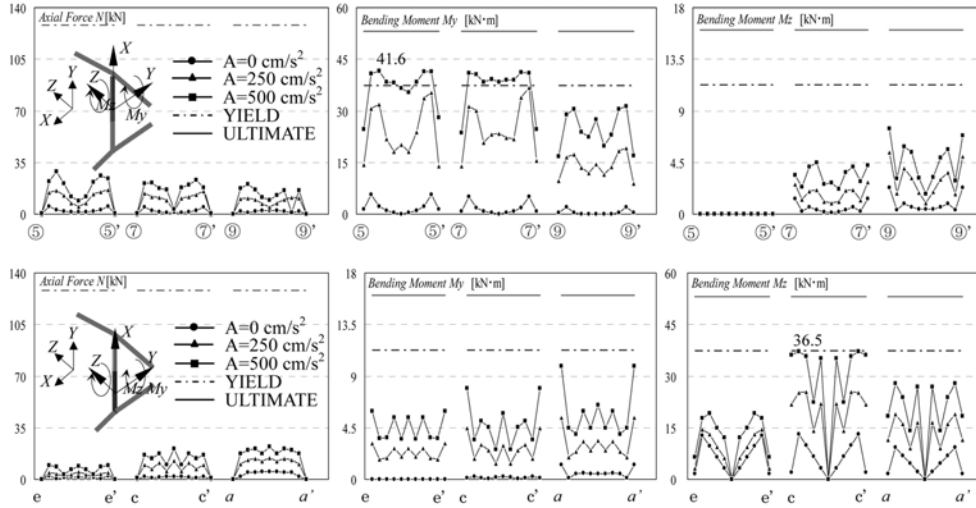


Fig. 16 Member Forces of The Selected Struts under Earthquake Motion in the Z Direction; (Upper: Left to Right) Upper Joint of Strut; Axial Forces, Bending Moment M_y , Bending Moment M_z (Lower: Left to Right) Lower Joint of Strut; Axial Forces, Bending Moment M_y , Bending Moment M_z

and struts during the earthquake given in the x and z directions respectively. As a general remark, it can be noticed that the struts have mainly absorbed the strain energy when the structure is subjected to the earthquake with maximum input acceleration $A_{max} = 500 \text{ cm/s}^2$, while for ground motion $A_{max} \leq 300 \text{ cm/s}^2$, most of the strain energy is absorbed by the arches. This phenomenon may be explained with regards to the structures performance at earthquake loading as follows. During a strong earthquake shaking, the plasticity will firstly occur at the strut joints by yielding. However the strain energy would be absorbed very well by these joints when yielding takes a place, reducing the possibility of some unexpected damages to the main arches. At weak earthquake, strain energy is mainly absorbed by the main arches; but as the deformations are quite small in this case, the main arches would be in safe condition.

4.2.7 Deformation due to shear force

The next behavior to be investigated is the deformation of the joints under shear forces of q_x and q_z .

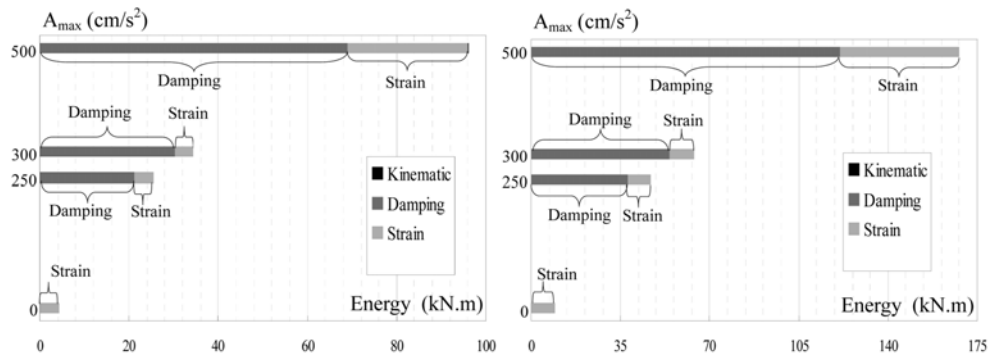


Fig. 17 Energy Descriptions; (a) Earthquake in the X Direction (left) and in the Z Direction (right)

For this purpose, a strut member located at the center of the dome is selected, and then the shear deformation (δ_x) of the upper joint under earthquake in the x direction and the shear deformation (δ_z) of the lower joint under earthquake in the z direction are described.

From Fig. 18, the largest sway of the upper joint of the selected strut under earthquake motion given in the x direction is about 4.0 cm (for $A_{max} = 500 \text{ cm/s}^2$). When the earthquake motion is given in the z direction with similar maximum acceleration $A_{max} = 500 \text{ cm/s}^2$, the lower joint is only deformed about 3.0 cm (see Fig. 19).

4.2.8 Residual Displacement

Fig. 20 shows the residual plastic y directional displacement of the strut joints once the structure is subjected to the earthquake motion. For the loading given in the x direction, the largest residual plastic y directional deformation occurs at the upper arch ⑨ - ⑨' is about 22.0 mm for $A_{max} = 500 \text{ cm/s}^2$ and at the lower arch $e - e'$ is about 13.0 mm. Comparing this value to the total maximum y directional displacement of the joint for similar A_{max} (Fig. 11), these displacements are reduced about 40% (from 38.0 mm to 22.0 mm) for the upper arch and about 39.3% (from 32.8 mm to 13.0 mm) for the lower arch.

In case of the earthquake motion given in the z direction, the largest residual plastic y directional deformations occur at the upper joint of the arch ⑤ - ⑤'. It is around 13.0 mm under maximum earthquake

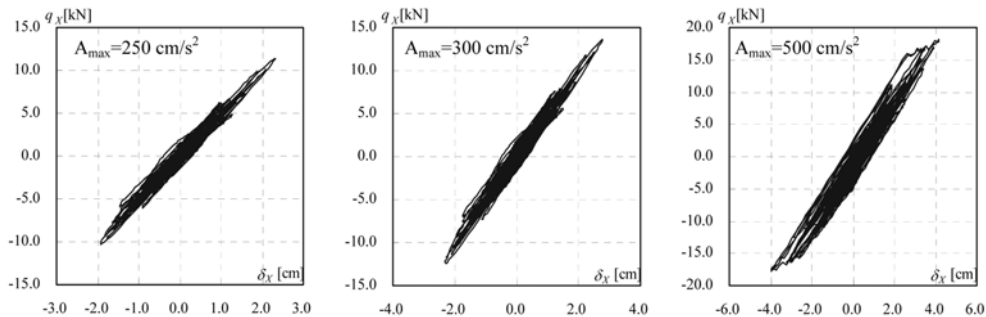


Fig. 18 Shear Deformation of the Upper Joint of Selected Arch Member under Earthquake in the X Direction (Left to Right) with $A_{max} = 250, 300, 500 \text{ cm/s}^2$

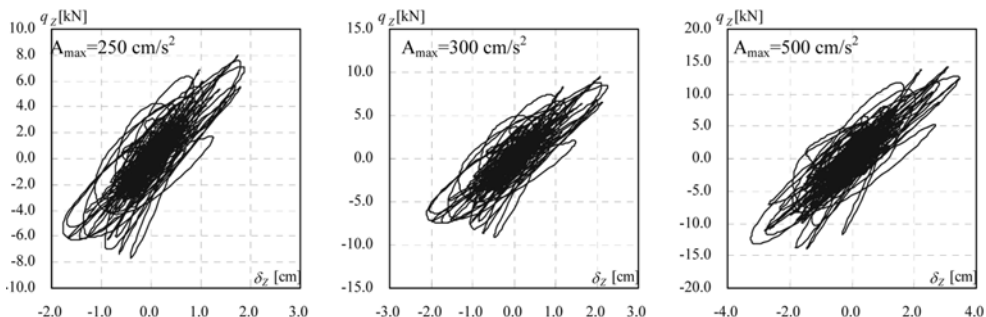


Fig. 19 Shear Deformation of the Lower Joint of Selected Arch Member under Earthquake in the Z Direction (Left to Right) with $A_{max} = 250, 300, 500 \text{ cm/s}^2$

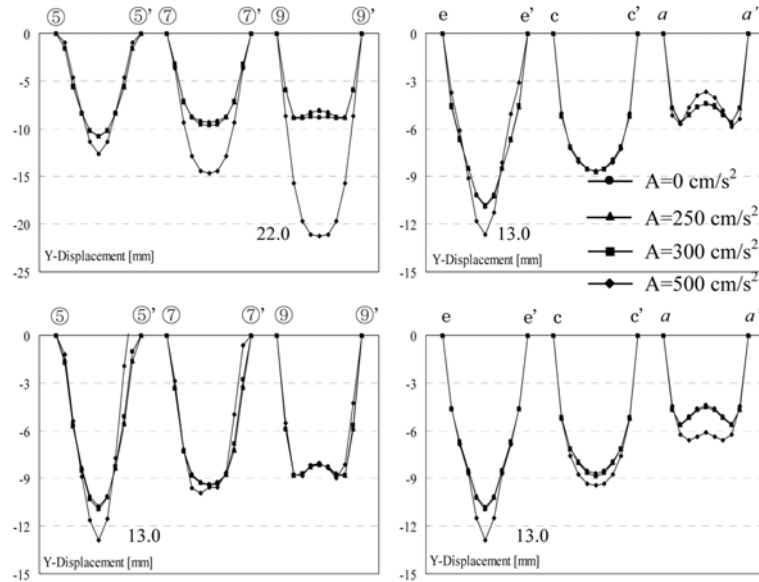


Fig. 20 Residual Plastic Y-Displacement of The Selected Arches (Upper - Left to Right) Upper and Lower Arches for Earthquake given in the X Direction (Lower - Left to Right) Upper and Lower Arches for Earthquake given in the Z Direction

acceleration $A_{max} = 500 \text{ cm/s}^2$. The displacement has been reduced by 81% (from 68.0 mm to 13.0 mm) when comparing this value to the total maximum y directional displacement of the joint (see Fig. 12). Similarly, the largest plastic deformation in the y direction is observed at lower joint of the arch $e - e'$, is about 13.0 mm and it shows about 65.0% reduction from the maximum total displacement (from 20.5 mm as shown in Fig. 12).

Briefly this study showed that; maximum residual plastic deformation at a node of the proposed dome under severe horizontal earthquake motion with higher maximum acceleration (example $A_{max} = 500 \text{ cm/s}^2$) is only about 20%-50% of the maximum total displacement. In general, these values are small enough and surprisingly resulted from the cases with $A_{max} = 500 \text{ cm/s}^2$. This fact proves the effectiveness of joint yielding in absorbing the strain energy when the structure is subjected to heavy dynamic loadings.

5. Discussion

5.1 Behavior of domes under horizontal earthquake motion

When the dome is loaded by earthquake motion horizontally in the x direction, the most significant nodal deformations as well as the nodal accelerations will occur in x direction at the upper joints of the struts. If loading is given in z direction, nodal deformations and nodal accelerations are again become significant in the direction of loading: i.e. z direction, but at the lower joints of the struts. The reason is mainly due to the geometrical factor. For the first case, the rigidity of the upper joints is smaller in x direction, and for the second case, rigidity of the lower joints is smaller in the z direction; resulting in significant deformation in the direction of small rigidity.

In this research, the maximum earthquake acceleration A_{max} is given in the range of 0 to 500 cm/s². Output results suggest that for the earthquake loading $A_{max} \leq 250$ cm/s², critical joints of the proposed dome could behave elastically. As shown in Figs. 15 and 16, the bending moments (M_y and M_z) of the joints are very much less than the yield moments. When A_{max} is increased to be $A_{max} = 500$ cm/s², the critical joints start to yield; giving maximum M_z of the lower joint as 42.5 kN.m (see Fig. 15) when the yield capacity $M_{y,IPB}$ is 37.24 kN.m (see Table 1). Similar result is observed for bending moment M_y of the upper joint (see Fig. 16). The remarkable finding of this system was the strain energy absorbing capability of joints of strut members at yielding failure. Fig. 17 indicates that joints of strut members efficiently absorb the strain energy (more than 75%) at high seismic loads, $A_{max} = 500$ cm/s². The residual plastic deformations (see Fig. 20) are much smaller than maximum deformations of the dome at severe earthquake loading (see Figs. 11 and 12). The characteristic found in this study is the T-joint of the struts may work as the energy absorbing devices. It reduces the risk of any heavy damage occurrence to the main arches of the dome, and joints of the struts act as a damage controller by absorbing the disturbances' energy. In general, these results imply a conclusion that the presented dome has a damage-control characteristic against severe earthquake motion leading a possibility for a new manner of structural design.

5.2. Behavior of domes under safety level

Now, we just focus our attention on behavior of the dome under the earthquake motion with a maximum acceleration of $A_{max} = 250$ cm/s²; an instance where the joint yielding is not occurred (see Figs. 15 and 16). The result shows that the maximum x deformation at the upper joint under the x directional earthquake loading is about 31.75 mm (see arch ⑨ - ⑨ of Fig. 11) and about 8.0 mm under the dead load (see Fig. 10). When the earthquake given in the z direction, a maximum z deformation of 32.60 mm at the lower joint (see arch $a - a'$ of Fig. 12) and very small deformation (about 1 mm) due to the dead load are occurred (see Fig. 10). These are in acceptable design level since the total elastic displacement due to both loads is only around 50 mm.

In the vertical direction, the maximum nodal acceleration for the earthquake with $A_{max} = 250$ cm/s² is 416 cm/s² for the upper joint (see arch ⑨ - ⑨ of Fig. 13) if the earthquake is given in the x direction; and it becomes 803 cm/s² for the lower joint (see arch c to c' of Fig. 14) if the earthquake is given in the z direction. Because of the dead load per node is equal to 10.62 kN (see Section 2.4) or 1082.56 kg as the dead mass, the maximum dynamic force for the former is equal to $P = 1082.56 \text{ kg} \times 4.16 \text{ m/s}^2 = 4503.45 \text{ N} = 4.5 \text{ kN}$ and the latter is $P = 1082.56 \text{ kg} \times 8.03 \text{ m/s}^2 = 8692.96 \text{ N} = 8.69 \text{ kN}$. Then, in a rough comparison of these values with the results of Fig. 6 implies that the forces are still lower than the static elasto-plastic buckling load of the proposed dome. Further, in term of displacements, the former has been vertically deformed around 18.0 mm due to dynamic load and around 8.0 mm due to dead load (see arch ⑨ to ⑨ of Figs. 11 and 10), while the latter has been vertically deformed around 45.9 mm due to dynamic load and 8.5 mm due to dead load (see arch c to c' of Figs. 12 and 10). These are acceptable since based on static analysis (see Section 3) the maximum acceptable deformation in the y direction is equal to $L_z / 300 = 200$ mm.

The maximum acceleration $A_{max} = 250$ cm/s² is just selected based on the condition that, no joint yielding occurred in the critical joints at that loading. However a further study to investigate the real acceleration limits for yielding and for the collapse need to be done. It is also important to offer some practical methods to predict these accelerations readily, without any complicated calculation, when the proposal to be used in practice.

6. Conclusion

The present paper has investigated the dynamic behavior of a new type of two-way single layer lattice dome with nodal eccentricity. The procedure is based on a dynamic eigenvalue analysis in investigating the mode shapes of deformation of the proposed domes under earthquake motion given horizontally in the x and z directions, and also based on elasto-plastic analysis for failure mechanism under severe earthquake motions. The presumptions assumed in the study are that (1) the plan for the roofs is rectangular with a size of $L_x \times L_z$, where L_x and L_z are 60 m, (2) the rise is relatively shallow with 30° and 25° for the half open angle respectively in the x and z directions, (3) the length of strut member placed between orthogonal arches is 250 cm, (4) the boundaries of dome at all peripheries are pin supported, and (5) the dead load is uniformly distributed.

Several important conclusions can be drawn as follows.

- Based on static elasto-plastic analysis, the proposed dome with geometrical imperfection (based on the first buckling mode) is capable to support any uniform vertical load up to $2.1P_0$ (where P_0 is the dead load of the structure) until it reached to yielding point.
- A dynamic eigenvalue analysis shows that the major deformation mode of the dome under earthquake motion is non-symmetrical in the x direction where the nodes at the upper arches seem to be largely deformed horizontally in the x direction, while nodes of lower arches are deformed in the both x and z directions. Moreover, the major deformation under earthquake motions in the z direction seems to be symmetry in z axis but not in x axis. The shapes of deformation are predominant in the x and y directions rather than in the z direction (the direction of earthquake motion).
- The benefit of using the T-joint struts against earthquake is that the yielding of strut joints has a good capability to absorb some of seismic energy against severe earthquakes; therefore any plastic residual deformations that occurred after the dynamic loads are much smaller than maximum deformation during the earthquake. The results are very beneficial to reduce any heavy damages to the main arches. Moreover, it implies that the proposed dome has a kind of damage-control characteristic against severe earthquake motion.
- Under earthquake motion with $A_{max} = 250 \text{ cm/s}^2$ the critical joints of the dome are remain in elastic condition. The total maximum x deformation of the upper joint is 53 mm under the earthquake motion given in the x direction, and becomes 41 mm when excitation is given in the z direction. In the vertical direction is much larger for the latter case, while the lower joint is deformed around 54.4 mm.
- The damage effect due to earthquake motion is not too significant under $A_{max} = 250 \text{ cm/s}^2$. Although above this value, the joints of strut members experience some kind of plastic deformation, the analysis shows that the global deformation may remain almost elastic with small residual displacements in the vertical direction even in case of large input of $A_{max} = 500 \text{ cm/s}^2$. The dynamic behavior implies that this kind of new single layer lattice dome has a fine feasibility of construction in seismic region.

Acknowledgement

The authors gratefully acknowledge for the partial supports as a Grand-in-Aid under grant No. (C)18560546 given by the Ministry of Education, Science, Sports and Culture of Japanese Government.

References

- Kato, S., Yamashita, T., Nakazawa, S., Kim, Y.B., Fujibayashi, A (2007); "Analysis based Evaluation for Buckling Loads of Two-Way Elliptic Paraboloidal Single Layer Lattice Domes", *J. Constr. Steel Res.*, **63**(9), 1219-1227.
- Kato, S., Satria, E., Nakazawa, S (2007), "Analysis Based Estimation of Buckling Strength of Two-Way Single Layer Lattice Dome with Semi Rigid Connection", *IASS Symposium, Shell and Spatial Structures*, Venice, Italy, CD-ROM Paper No. 138T9, December.
- Kurokawa, Y., Yamada, T., Yoshida, A., Ikeda, Y. (1988), "Study on Space Frame by 3-Dimensional Tubular Rahmen: (Part-1) Frame Structure Analysis of Akita Ground", *AIJ Annual Meeting*, Vol-B1, pp.167-168 (in Japanese).
- Ishii, K (1995), "Membrane Structures in Japan", *SPS Publishing Company*, Tokyo.
- Narayanan S. (2006), "Space Structures: Principles and Practice", Multi-Science Publishing Co. Ltd. UK.
- Fentiman, H.G (1984), "International Examples of Latticed Triodetic Structures", Proceeding of the Third International Conference on Space Structures, Guildford, UK, September, pp. 9-14.
- Escrig, F., Sanchez, J. (2001), "Great Space Curved Structures with Rigid Joints", *International Symposium on Theory, Design and Realization of Shell and Spatial Structures*, Nagoya, Japan, October, pp.292-293.
- Escrig, F., Sanchez, J. (2004), "A New Roof Grid to Cover a Large Area: The Vierendeel Solution", *Int. J. Space Struct.*, June, **19**(4), 177-194.
- Kato, S., Satria, E., Nakazawa, S (2007), "Buckling Analysis of Two-Way Single Layer Lattice Dome with Nodal Eccentricity", *IASS Symposium, Shell and Spatial Structures*, Venice, Italy, CD-ROM Paper No. 284T9, December.
- Kato, S., Satria, E., Kim, Y.B., Nakazawa, S. (2008), "Analysis of Nonlinear Behavior and Feasibility for A New Type of Two-Way Single Layer Lattice Dome with Nodal Eccentricity using T-Joint Struts", *J. Jap. Society Steel Constr. (JSSC)*, June, **15**(58), 21-36.
- Satria, E., Kato, S., Nakazawa, S., Kakuda, D. (2008), "Buckling Behavior of Two-Way Single Layer Lattice Dome with Nodal Eccentricity", *J. Struct. Eng.*, Architectural Institute of Japan (AIJ), March, **54B**, 679-692.
- Soong, T.T., Spencer Jr, B.F. (2002), "Supplemental Energy Dissipation: State-of-the-Art and State-of-the-Practice", *Eng. Struct.*, **24**(3), 243-259.
- Di Sarno, L., Elnashai, A.S. (2005), "Innovative Strategies for Seismic Retrofitting of Steel and Composite Structures", *Pro. Struct. Eng. Mat.*, May, **7**(3), 115-135.
- Tatemichi, I., Kawaguchi, M. (2000), "A New Approach to Seismic Isolation: Possible Application in Space Structures", *Int. J. Space Struct.*, May, **15**(2), 145-154.
- Hitomi, Y., Osawa, K., Nakagawa, K., Saitoh, M. (2001), "Structural Design of the Yamaguchi Dome", *International Symposium on Theory, Design and Realization of Shell and Spatial Structures*, Nagoya, Japan, October, pp. 292-293.
- Fan, F., Shen, S.Z., Parke, G.A.R. (2004), "Theoretical and Experimental Study of Vibration Reduction in Braced Domes using a Viscous Damper System", *Int. J. Space Struct.*, December, **19**(4), 195-202.
- Kato, S., Kim, Y.B., Nakazawa, S., Ohya, T (2006), "Simulation of the Cyclic Behavior of J-Shaped Steel Hysteresis Devices and Study on the Efficiency for Reducing Earthquake Responses of Space Structures", *J. Constr. Steel Res.*, **61**(10), 1457-1473.
- Kato, S., Nakazawa, S., (2000), "Seismic Design Method of Single Layer Reticular Domes with Braces Subjected to Severe Earthquake Motions", *Sixth Asian Pacific Conference on Shell and Spatial Structures*, Seoul, Korea, October, pp. 131-140.
- Kato, S., Konishi, Y. (2001), "A Study on Behavior of A Double Layer Dome with VED Installed in the Braces of the Sub-Structures under Severe Earthquake Motions", *Int. Symposium on Theory, Design and Realization of Shell and Spatial Structures*, Nagoya, Japan, October, pp. 264-265.
- Fujita, M., Sedo, H., Iwata, M. (2002), "Flat System Truss with Axial Hysteretic Dampers as Damage-Controlled Structure", *J. Struct. Constr. Eng.*, AIJ, September, **559**, 165-172 (in Japanese).
- Ciampi, V., Ferreti, S.A. (1990), "Energy Dissipation in Building using Special Bracing System", *Proceeding of 9th European Conference on Earthquake Engineering*, Vol. 3, Moscow, pp. 9-18.
- Jurukovski, D., Petkovski, M., Rakicevic, Z. (1995), "Energy Absorbing in Regular and Composite Steel Frame

- Structures”, *Eng. Struct.*, June, **17**(5), 319 -333.
- Sabouri-Ghomi, S., Roufegarinejad, A. (2005), “Nonlinear Behavior of Yielding Damped Braced Frames”, *The Structural Design of Tall and Special Buildings*, October, **14**(1), 37-45.
- Satish Kumar, S.R., Prasada Rao, D.V. (2006), “RHS Beam to Column Connection with Web Opening – Experimental Study and Finite Element Modelling”, *J. Constr. Steel Res.*, August, **62**(8), 739-746.
- Jin, J., El-Tawil, S. (2005), “Seismic Performance of Steel Frames with Reduced Beam Section”, *J. Constr. Steel Res.*, April, **61**(4), 453-471.
- Wilkinson, S., Hurdman, G, Crowther, A. (2006), “A Moment Resisting Connection for Earthquake Resistant Structures”, *J. Constr. Steel Res.*, March, **62**(3), pp. 295-302.
- Kato, S., Yamashita, T. (2002); “Evaluation of Elasto-Plastic Buckling Strength of Two-Way Grid Shells using *Continuum Analogy*”, *Int. J. Space Struct.* December, **17**(4), 249-261.
- Kato, S., Yamauchi, Y., Ueki, T., Okuhira, K. (2005), “Buckling Load of Elliptic Paraboloidal Single Layer Reticulated Roofs with Simple Supports under Uniform Load”, *Int. J. Space Struct.*, December, **20**(4), pp. 211-224.
- Lopez, A, Puente, I, Serna, M.A. (2007); “Direct Evaluation of the Buckling Loads of Semi-Rigidly Jointed Single Layer Latticed Domes under Symmetric Loading”, *Eng. Struct.*, January, **29**(1), 101-109.
- Balut, N.; Gioncu, V. (2000); “The Influence of Geometrical Tolerances on the Behavior of Space Structures”, *Int. J. Space Struct.*, December, **15**(3-4), 189-194.
- Architectural Institute of Japan (1990), “Recommendation for the Design & Fabrication of Tubular Structure in Steel”, Maruzen, Tokyo (in Japanese).
- Architectural Institute of Japan (1993), “*Japanese Architectural Standard Specification JASS 6 Steel Work*”, Maruzen, Tokyo (in Japanese)..
- Architectural Institute of Japan (2002), “*Design Standard for Steel Structures*”, Maruzen, Tokyo (in Japanese).